Theory of Raman scattering from Leggett's collective mode in a multiband superconductor: Application to MgB_2

M. V. Klein
Department of Physics and Frederick Seitz Materials Research Laboratory, University of Illinois at Urbana-Champaign, Urbana, Illinois 61801, USA
(Received 13 May 2010; published 7 July 2010)

In 1966, Leggett used a two-band superconductor to show that a new collective mode could exist at low temperatures, corresponding to a counterflow of the superconducting condensates in each band. Here, the theory of electronic Raman scattering in a superconductor by Klein and Dierker (1984) is extended to a multiband superconductor. Raman scattering creates particle/hole (p/h) pairs. In the relevant A_{1g} symmetry, the attraction that produces pairing necessarily couples excitations of superconducting pairs to these p/h excitations. In the Appendix, it is shown that for zero wave-vector transfer q, this coupling modifies the Raman response and makes the long-range Coulomb correction null. The two-band result is applied to MgB_2 where this coupling activates Leggett's collective mode. His simple limiting case is obtained when the interband attractive potential is decreased to a value well below that given by local-density approximation (LDA) theory. The peak from Leggett's mode is studied as the potential is increased through the theoretical value. With realistic MgB_2 parameters, the peak broadens through decay into the continuum above the smaller (π band) superconducting gap. Finite q effects are also taken into account, yielding a Raman peak that agrees well in energy with the experimental result by Blumberg *et al.* [Phys. Rev. Lett. **99**, 227002 (2007)]. This approach is also applied to the $q=0$, two-band model of the Fe pnictides considered by Chubukov *et al.* [Phys. Rev. B **79**, 220501(R) (2009)].

DOI: 10.1103/PhysRevB.82.014507 PACS number(s): 74.70.Ad, 74.25.Gz

I. INTRODUCTION

In a superconductor, a longitudinal density oscillation corresponds to an oscillation of the phase of the superconducting order parameter. As shown by Bogolyubov *et al.*[1] and Anderson,[2] this oscillation would amount to a collective mode with zero energy at zero wave vector in the absence of the long-range Coulomb interaction between the conduction electrons. The presence of this interaction, however, causes the condensate density oscillation to become the electronic plasma oscillation, typically with an energy of 5–10 eV. Leggett showed that for a simple model of a two-band superconductor, it could be possible for the superconducting condensates in each band to oscillate longitudinally relative to one another, equivalent to an oscillation in the relative phase of the two condensates, with the net displacement of the total condensate being zero.[3] The frequency of this mode and its dispersion with wave vector q would depend substantially on the effective interband pairing potential. If this potential were sufficiently small, but not zero, the small q mode frequency would be less than the smaller of the superconducting gaps 2Δ, for the two bands. In the low-temperature limit, this mode would become a true collective mode with an infinite lifetime.

There is good evidence that MgB_2 is a multiband superconductor. Whereas theory suggests that there are two bands primarily of $2p\sigma$ character and two bands of $2p\pi$ character,[4] most experimental superconducting properties can be described as though there were one σ band and one π band.[5] The σ band is nearly two dimensional. Its barrel-shaped Fermi surface is almost cylindrically symmetric about the c axis and the c-axis component of the Fermi velocity is very small. On the other hand, the π-band Fermi surface is three dimensional. On it the root-mean-square Fermi velocity components are large and nearly isotropic.

Electronic Raman-scattering measurements in E_{2g} symmetry ($xx-yy$ or xy) show two features due to superconductivity: a relatively sharp peak at $2\Delta_\sigma=13.5$ meV associated with the σ band and an onset without a peak at $2\Delta_\pi=4.6$ meV associated with the π band.[6] As shown by Blumberg *et al.*, the situation is different for Raman in the fully symmetric A_{1g} symmetry ($xx+yy$).[7] Apart from two-phonon features, an electronic Raman peak was found at 9.4 meV, midway between the onset of the π-band continuum at $2\Delta_\pi$ and the σ-band peak at $2\Delta_\sigma$. Because it can decay into the π-band continuum, the mode signified by this peak cannot be a true collective mode. We will show that it represents a resonance mode that follows by continuity from Leggett's collective mode when allowance is made for (1) a vertex correction that is related to the mechanism that allows electronic Raman scattering to couple to it, (2) damping due to decay into the π band continuum, (3) necessary kinematic corrections that depend on $\boldsymbol{q}\cdot\boldsymbol{v}_F$, where $\boldsymbol{q}$ is the transferred wave vector and $\boldsymbol{v}_F$ is the Fermi velocity vector, and (4) integration over values of q that are ill defined due to optical absorption, all using a realistic set of physical parameters that apply to MgB_2.

The present work is based on a paper by Klein and Dierker (K-D) (Ref. 8) that uses a Green's-function approach to describe the electronic Raman response function as resulting from Kawabata's four-vertex function.[9] The latter may be collapsed into a two-vertex polarization "bubble." The bare vertex γ_k comes from the electron-photon interaction and is the sum of two terms: the A^2 term, where $\boldsymbol{A}$ is the vector potential, couples to the electron-density operator in first order and the $\boldsymbol{p}\cdot\boldsymbol{A}$ term couples in second order ($\boldsymbol{p}$ is the elec-

tron momentum operator) to a densitylike quantity through a virtual intermediate state. The sum of these terms, γ_k, gives the amplitude for excitation from near the FS to near the FS of an electron from wave vector $\boldsymbol{k}$ to wave vector $\boldsymbol{k}+\boldsymbol{q}$ while the incident laser (L) photon is transformed into the scattered (S) photon with respective wave vector and energy transfers $\boldsymbol{q}=\boldsymbol{k}_L-\boldsymbol{k}_S$ and $\omega=\omega_L-\omega_S$. For small values of q relative to the Fermi wave vector, the vertex γ_k does not depend on $\boldsymbol{q}$. Due to the $\boldsymbol{p}\cdot\boldsymbol{A}$ term, γ_k will depend on ω_L when the excitation energy to the intermediate state comes into resonance with ω_L. Such resonance Raman effects are probably not relevant for the Blumberg *et al.* data taken with 1.65 eV laser light. Optical data[10] and band-structure calculations[4] show that interband optically allowed transitions to and from the Fermi surface in MgB_2 occur at energies well above 1.65 eV. The "mass approximation" for the relevant A_{1g} symmetry may then be applied. It says that the electronic Raman vertex γ_k is r_o, the classical radius of the electron, multiplied by $[\mu_{xx}(k)+\mu_{yy}(k)]$, where $\boldsymbol{\mu}(k)$ is the inverse effective mass tensor at wave vector k near the FS. The holelike σ band and the electronlike π band possess $\mu_{xx}+\mu_{yy}$ values that have opposite signs.

To allow for the possibility of electronic resonance(s) with intermediate state(s), we assume in our derivation that γ_k is complex due to the appearance of an imaginary term in the energy denominator(s) proportional to the inverse lifetime of the intermediate state(s).

II. MODEL AND ITS EQUATIONS

To carry out the calculation, we will set up the problem in a more general fashion and then make the assumption that γ_k is a positive constant for k in the π band and a negative constant for k in the σ band. These bare vertices create a positive charge-density (particle/hole or p/h) excitation of wave vector $\boldsymbol{q}$ in the π band and a negative charge-density excitation of wave vector $\boldsymbol{q}$ in the σ band. In the Nambu formalism[11] used by K-D, these p/h excitations are associated with the τ_3 Nambu matrix. A generalized vertex equation necessarily couples the (p/h) τ_3 channel with the particle/particle (p/p) τ_2 (phase) channel that describes excitations of the condensate. This is the first of four final-state corrections to be consider in this paper, the pairing correction. The opposite signs of the bare γ_k in the p/h channel produce opposite forcing terms in the p/p-phase channel for the two bands and thus enable coupling to Leggett's collective mode. The dynamics of the mode are altered because of the second final-state correction that occurs in the p/h channel, the "vertex correction."

We begin by quoting key results from Secs. III.2 and III.3 of K-D, somewhat rewritten to fit our present needs. We assume that $\boldsymbol{k}$, hereafter denoted by k, is a wave vector near the Fermi surface, referring to one or more bands, and consider a k-dependent superconducting gap Δ_k, normal-state energy minus the Fermi energy ε_k, and Fermi velocity $\boldsymbol{v}_k=\boldsymbol{\nabla}_k\varepsilon_k$. Define

$$\beta_k \equiv \sqrt{\frac{\omega^2-(\boldsymbol{q}\cdot\boldsymbol{v}_k)^2}{4\Delta_k^2}}; \quad f_k(\omega,\boldsymbol{q}) \equiv \frac{\arcsin\beta_k}{\beta_k\sqrt{1-\beta_k^2}}, \tag{1}$$

$$p_k(\omega,\boldsymbol{q}) \equiv f_k(\omega,\boldsymbol{q})\left[1-\left(\frac{\boldsymbol{q}\cdot\boldsymbol{v}_k}{\omega}\right)^2\right], \tag{2}$$

$$r_k(\omega,\boldsymbol{q}) \equiv \frac{f_k(\omega,\boldsymbol{q})\omega^2-(\boldsymbol{q}\cdot\boldsymbol{v}_k)^2}{\omega^2-(\boldsymbol{q}\cdot\boldsymbol{v}_k)^2}. \tag{3}$$

The correct branches of the square root and arcsin functions are obtained by adding an infinitesimal positive imaginary part to the frequency variable ω, which is itself assumed to be positive, and by assuming that branch cuts are along the negative real axis of the arguments of the two functions. Note that when $\boldsymbol{q}=0$, p_k and r_k equal f_k but when $\boldsymbol{q}\neq 0$, they no longer equal f_k.

Assume zero temperature and that a nonretarded effective potential $D^{(p)}_{k,k'}$ (pairing correction) acts between a p/p pair at k and one at k' and that a potential $D^{(v)}_{k,k'}$ (vertex correction) acts between a p/h pair at k and one at k'. We obtain the two vertex equations, rearranged from K-D Eqs. (10a) and (10b), that connect the "dressed" vertices $\Gamma^{(3)}_k$ and $\Gamma^{(2)}_k$ for the p/h and p/p-phase channels, respectively, with the bare p/h vertex γ_k,

$$\Gamma^{(3)}_k = \gamma_k + \int dS_{k'} D^{(v)}_{k,k'} \frac{i\omega}{2\Delta_{k'}}\left[f_{k'}\Gamma^{(2)}_{k'} - \frac{2i\Delta_{k'}}{\omega} r_{k'}\Gamma^{(3)}_{k'}\right], \tag{4}$$

$$\Gamma^{(2)}_k = -\int dS_{k'} D^{(p)}_{k,k'} L_{k'}\Gamma^{(2)}_{k'} - \int dS_{k'} D^{(p)}_{k,k'} \frac{\omega^2}{4\Delta^2_{k'}} \times\left[p_{k'}\Gamma^{(2)}_{k'} - \frac{2i\Delta_{k'}}{\omega} f_{k'}\Gamma^{(3)}_{k'}\right]. \tag{5}$$

Here $dS_k=(2\pi)^{-3}d^3k\,\delta(\varepsilon_k)$ and the Dirac delta function $\delta(\varepsilon_k)$ forces the k integral to be over the Fermi surface. $L_k \equiv \sinh^{-1}(\omega_k/\Delta_k)$ is a loglike term involving a cutoff energy ω_k and the gap. It also occurs in the BCS-type equation for the gap, K-D Eq. (18),

$$\Delta_k = -\int dS_{k'} D^{(p)}_{k,k'} L_{k'}\Delta_{k'}. \tag{6}$$

Also needed is the equation for the polarization bubble, or Raman response function, rearranged from K-D Eq. (10c),

$$B_{\gamma',\Gamma\gamma}(\omega,\boldsymbol{q}) = -2\int dS_k \gamma'_k \frac{i\omega}{2\Delta_k}\left[f_k\Gamma^{(2)}_k - \frac{2i\Delta_k}{\omega} r_k\Gamma^{(3)}_k\right]. \tag{7}$$

Here the notation $B_{\gamma',\Gamma\gamma}(\omega,\boldsymbol{q})$ means that the bare vertices are γ_k and γ'_k, with γ_k dressed by vertex corrections. The argument $(\omega,\boldsymbol{q})$ refers the fact that f_k, p_k, r_k, and $\Gamma^{(2,3)}_k$ depend on the same argument, omitted here for simplicity. The factor of 2 outside the integral is from a summation over spin inherent in the Nambu formalism.

In general, vertex corrections result from an infinite sum of ladder diagrams. This has the consequence that the result is symmetric in the two vertices. Thus[12]

$$B_{\gamma',\Gamma\gamma}(\omega,\boldsymbol{q}) = B_{\gamma,\Gamma\gamma'}(\omega,\boldsymbol{q}). \tag{8}$$

Next we make the third final-state correction by correcting the response function for the long-range Coulomb interac-

tion, K-D Eq. (17), to obtain the screened response function,

$$B_{\gamma^*,\Lambda\gamma}(\omega,\boldsymbol{q}) = B_{\gamma^*,\Gamma\gamma}(\omega,\boldsymbol{q}) + \frac{B_{\gamma^*,\Gamma 1}(\omega,\boldsymbol{q})V_q B_{1,\Gamma\gamma}(\omega,\boldsymbol{q})}{1 - V_q B_{1,\Gamma 1}(\omega,\boldsymbol{q})} \tag{9a}$$

and with

$$V_q \equiv \frac{4\pi e^2}{q^2 v_c}. \tag{9b}$$

Here v_c is the volume of a unit cell. For values of q that are small compared to the inverse lattice constant,

$$B_{\gamma^*,\Lambda\gamma}(\omega,\boldsymbol{q}) \to B_{\gamma^*,\Gamma\gamma}(\omega,\boldsymbol{q}) - \frac{B_{\gamma^*,\Gamma 1}(\omega,\boldsymbol{q})B_{1,\Gamma\gamma}(\omega,\boldsymbol{q})}{B_{1,\Gamma 1}(\omega,\boldsymbol{q})}. \tag{10}$$

The appearance of 1 on the right side of these equations signifies that the relevant bare vertex is unity, 1, for all values of k. On the right side of Eq. (10), the second term, the so-called "screening correction," projects off, in a $\boldsymbol{q}$- and ω-dependent fashion, from the bare vertex γ_k that portion parallel to 1. When $\gamma_k \propto 1$, the projection cancels the first term, and the screened response function is zero.

III. DEALING WITH THE SPREAD IN WAVE VECTOR DUE TO OPTICAL ABSORPTION

The photon wave vectors are proportional to the complex index of refraction. Thus, for Raman scattering from metals, the wave-vector transfer is a complex quantity $q=q'+iq''$. The experiments of Blumberg *et al.*[7] were such that $\boldsymbol{q}$ was parallel to the hexagonal symmetry axis. If z denotes the distance along the axis measured from the sample surface, then the perturbation that drives the Raman response has spatial dependence $e^{i(q'+iq'')z}$. This has a Fourier coefficient $(i/[\sqrt{2\pi}(q'+iq''-q)]$. The optical penetration depth, $(2q'')^{-1}$, is on the order of 1/10th the wavelength of light and thus much larger than a lattice constant. Therefore, Raman is essentially a bulk probe, and excitations with different wave vectors q are independent, that is, noninterfering. The physical screened response function is obtained by integrating $B_{\Lambda(\gamma),\gamma^*}(\omega,q)|1/[\sqrt{2\pi}(q'+iq''-q)]|^2$ over q from $-\infty$ to ∞. The Raman intensity $I(\omega)$ is minus the imaginary part of the result. Using the fact that $B_{\gamma^*,\Lambda_\gamma}(\omega,q)$ is even in q, we obtain a result equivalent to K-D's Eq. (4),

$$I(\omega) = -\int_0^\infty \frac{\mathrm{Im}[B_{\gamma^*,\Lambda\gamma}(\omega+i0^+,q)](q'^2+q''^2+q^2)dq}{\pi[(q'^2+q''^2+q^2)^2-4q^2q'^2]}. \tag{11}$$

IV. APPLICATION TO THE MULTIBAND CASE: SIMPLIFYING ASSUMPTIONS

We introduce j as a band index and k_j to denote wave-vector values in band j. The superconducting gap Δ_j and the magnitude of the Fermi velocity v_j are assumed to be constants in each band. Let u denote the cosine of the angle between the direction of $\boldsymbol{q}$ and the direction of the Fermi velocity $\boldsymbol{v}_{k_j}$ at k_j. The quantities appearing in Eqs. (1)–(3) will depend on the discrete variable j and the continuous variable u,

$$\beta_k \to \beta_j(\omega,q,u) \equiv \sqrt{\frac{\omega^2-(qv_ju)^2}{4\Delta_j^2}}, \tag{12}$$

$$f_k \to f_j(\omega,q,u) \equiv \frac{\arcsin\,\beta_j(\omega,q,u)}{\beta_j(\omega,q,u)\sqrt{1-\beta_j(\omega,q,u)^2}}, \tag{13}$$

$$p_k \to p_j(\omega,q,u) \equiv f_j(\omega,q,u)\left[1-\left(\frac{qv_ju}{\omega}\right)^2\right], \tag{14}$$

$$r_k \to r_j(\omega,q,u) \equiv \frac{f_j(\omega,q,u)\omega^2-(qv_ju)^2}{\omega^2-(qv_ju)^2}. \tag{15}$$

For n bands, the effective pairing potential is assumed to be represented by a symmetric $n\times n$ matrix $\boldsymbol{D}^{(p)}$ with elements $D^{(p)}_{j,j'}$ when k is in band j and k' is in band j'. Let the symmetric $n\times n$ matrix $\boldsymbol{D}^{(v)}$ denote the effective potential in the p/h channel responsible for vertex corrections and allow for the possibility that $\boldsymbol{D}^{(p)} \neq \boldsymbol{D}^{(v)}$. With these assumptions, the integrals in Eqs. (4)–(7) simplify into sums over band index j of integrals over the Fermi surface of that band, where the only variable in the integrand is u. The integral Eqs. (4) and (5) turn into discrete equations for the dressed vertices,

$$\Gamma_k^{(2,3)} \to \Gamma_j^{(2,3)}(\omega,q). \tag{16}$$

Upon introduction of the density of states ρ_j for band j, the integrals appearing on the right side of Eqs. (4)–(7) reduce to ρ_j multiplied by an average over u. Let $F_j(\omega,q)$, $P_j(\omega,q)$, and $Q_j(\omega,q)$ denote these averages of $f_j(\omega,q,u)$, $p_j(\omega,q,u)$, and $r_j(\omega,q,u)$, respectively. Make n vectors $\boldsymbol{F}(\omega,q)$, $\boldsymbol{P}(\omega,q)$, and $\boldsymbol{Q}(\omega,q)$ out of them, as well as n vectors out of ρ_j, Δ_j, L_j, bare vertices γ_j and dressed vertices $\Gamma_j^{(2,3)}(\omega,q)$. For simplicity, we will often drop the explicit dependence on (ω,q). Let $\boldsymbol{I}$ denote the n-dimensional unit matrix. The dot $\cdot$ denotes the scalar product of two vectors or matrix multiplication.

The existence of Leggett's mode requires the existence of the inverse,[13]

$$\boldsymbol{W} \equiv (\boldsymbol{D}^{(p)})^{-1}. \tag{17}$$

The following matrix equations were obtained. The explanation immediately follows

$$\boldsymbol{\Gamma}^{(3)} = \boldsymbol{\gamma} + \boldsymbol{D}^{(v)} \cdot \frac{i\omega}{2\boldsymbol{\Delta}}\left[\boldsymbol{F}\boldsymbol{\Gamma}^{(2)} - \frac{2i\boldsymbol{\Delta}}{\omega}\boldsymbol{Q}\boldsymbol{\Gamma}^{(3)}\right]\boldsymbol{\rho}, \tag{18}$$

$$\boldsymbol{W}\cdot\boldsymbol{\Gamma}^{(2)} = -\boldsymbol{L}\boldsymbol{\rho}\boldsymbol{\Gamma} - \frac{\omega^2}{4\boldsymbol{\Delta}^2}\left[\boldsymbol{P}\boldsymbol{\Gamma}^{(2)} - \frac{2i\boldsymbol{\Delta}}{\omega}\boldsymbol{F}\boldsymbol{\Gamma}^{(3)}\right]\boldsymbol{\rho}, \tag{19}$$

$$\boldsymbol{W}\cdot\boldsymbol{\Delta} = -\boldsymbol{L}\boldsymbol{\rho}\boldsymbol{\Delta}, \tag{20}$$

$$B_{\gamma^*,\Lambda\gamma}(\omega,q) = -2\boldsymbol{\gamma}' \cdot \frac{i\omega}{2\boldsymbol{\Delta}}\left[\boldsymbol{F}\boldsymbol{\Gamma}^{(2)} - \frac{2i\boldsymbol{\Delta}}{\omega}\boldsymbol{Q}\boldsymbol{\Gamma}^{(3)}\right]\boldsymbol{\rho}. \quad (21)$$

Equations (18) and (21) are matrix versions of Eqs. (4) and (7). Equations (19) and (20) were obtained by left multiplying the matrix equations we obtain from Eqs. (5) and (6) by $\boldsymbol{W}$. Above, when we write, e.g., $\boldsymbol{L}\boldsymbol{\rho}\boldsymbol{\Gamma}^{(2)}$, we refer to the n vector with components $L_j\rho_j\Gamma_j^{(2)}$.

Using the result $\boldsymbol{L}\boldsymbol{\rho}=-\boldsymbol{\Delta}^{-1}\boldsymbol{W}\cdot\boldsymbol{\Delta}$ from Eq. (20) to eliminate $\boldsymbol{L}\boldsymbol{\rho}$ from the first term on the right side of Eq. (19), we solve for $\boldsymbol{\Gamma}^{(2)}$ in terms of $\boldsymbol{\Gamma}^{(3)}$. After inserting the result in Eq. (18) and solving for $\boldsymbol{\Gamma}^{(3)}(\omega,q)$ in terms of $\boldsymbol{\gamma}$, we obtain from Eq. (21),

$$B_{\gamma',\Gamma\gamma}(\omega,q) = \boldsymbol{\gamma}' \cdot \boldsymbol{R}^{(p,v)}(\omega,q) \cdot \boldsymbol{\gamma}. \quad (22)$$

Here $\boldsymbol{R}^{(p,v)}(\omega,q)$ is the response-function matrix in the presence of vertex corrections due to pairing (p) and the vertex correction (v) due to the residual interaction in the particle/hole channel,

$$\boldsymbol{R}^{(p,v)}(\omega,q) = \frac{\boldsymbol{I}}{[\boldsymbol{R}^{(p)}(\omega,q)]^{-1} + \frac{1}{2}\boldsymbol{D}^{(v)}}, \quad (23)$$

where $\boldsymbol{R}^{(p)}(\omega,q)$ is the response-function matrix with a correction only due to pairing,

$$\boldsymbol{R}^{(p)} = -2\left[\|\boldsymbol{Q}\boldsymbol{\rho}\| + \|\boldsymbol{F}\boldsymbol{\rho}\| \cdot \frac{\boldsymbol{I}}{\frac{4}{\omega^2}\boldsymbol{U} - \|\boldsymbol{P}\boldsymbol{\rho}\|} \cdot \|\boldsymbol{F}\boldsymbol{\rho}\|\right]. \quad (24)$$

Above, dependence on (ω,q) remains understood, and $\|\boldsymbol{Q}\boldsymbol{\rho}\|$, $\|\boldsymbol{F}\boldsymbol{\rho}\|$, and $\|\boldsymbol{P}\boldsymbol{\rho}\|$ denote $n\times n$ diagonal matrices with components $Q_j(\omega,q)\rho_j$, etc., on the diagonal. The symmetric matrix

$$\boldsymbol{U} \equiv -\boldsymbol{\Delta}[\boldsymbol{W}\boldsymbol{\Delta} - (\boldsymbol{W}\cdot\boldsymbol{\Delta})\boldsymbol{I}], \quad (25)$$

or, in component form

$$U_{ij} = -\Delta_i\left(W_{ij}\Delta_j - \sum_{k=1}^{n} W_{ik}\Delta_k\delta_{ij}\right) \quad (26)$$

imprints on the matrices $\boldsymbol{R}^{(p)}(\omega,q)$ and $\boldsymbol{R}^{(p,v)}(\omega,q)$ the effect of the vertex correction due to pairing. $\boldsymbol{U}$ has the property that the elements in a given row or column sum to zero. Recalling $\mathbf{1}$, the n vector consisting of 1's, this property implies $\boldsymbol{U}\cdot\mathbf{1}=\mathbf{1}\cdot\boldsymbol{U}=0$.

Our fourth correction for final-state interactions will result by summing bubble diagrams consisting of the response-function matrix $\boldsymbol{R}^{(p,v)}(\omega,q)$ connected by a symmetric interaction matrix that we will denote by $\boldsymbol{D}^{(b)}$.[14] For clarity, we consider the possibility that $\boldsymbol{D}^{(b)}\neq\boldsymbol{D}^{(v)}\neq\boldsymbol{D}^{(p)}$. The series $\boldsymbol{R}^{(p,v)}(\omega,q)+\boldsymbol{R}^{(p,v)}(\omega,q)\cdot\boldsymbol{D}^{(b)}\cdot\boldsymbol{R}^{(p,v)}(\omega,q)+\cdots$ may be summed. The result, together with Eq. (23), gives a new response-function matrix $\boldsymbol{R}^{(p,v,b)}(\omega,q)$ obeying

$$\boldsymbol{R}^{(p,v,b)} = \frac{\boldsymbol{I}}{[\boldsymbol{R}^{(p)}]^{-1} + \frac{1}{2}\boldsymbol{D}^{(v)} - \boldsymbol{D}^{(b)}}. \quad (27)$$

The screened response function $\chi_\gamma(\omega,q)\equiv B_{\gamma^*,\Lambda\gamma}(\omega,q)$ then becomes

$$\chi_\gamma(\omega,q) = \boldsymbol{\gamma}^*\cdot\boldsymbol{R}\cdot\boldsymbol{\gamma} - \frac{(\boldsymbol{\gamma}^*\cdot\boldsymbol{R}\cdot\mathbf{1})(\mathbf{1}\cdot\boldsymbol{R}\cdot\boldsymbol{\gamma})}{\mathbf{1}\cdot\boldsymbol{R}\cdot\mathbf{1}} \quad (28)$$

with $\boldsymbol{R}=\boldsymbol{R}^{(p,v,b)}(\omega,q)$.

As discussed in the Appendix, the screening correction, the second term, vanishes as $q\to 0$.

V. TWO-BAND CASE WITH ZERO WAVE VECTOR

The remaining discussion concerns the case of $n=2$. Using the above assumption that $\boldsymbol{D}^{(p)}$ has an inverse [and thus the determinant $D_{11}^{(p)}D_{12}^{(p)}-(D_{12}^{(p)})^2$ is nonzero], we write the $q=0$ result for two bands as follows. [It can also be written in the form of the expression given in Eqs. (3), (5), and (6) of Blumberg *et al.*[7] but generalized to include the bubble diagrams.]

$$\chi_\gamma(\omega,q=0) = \frac{-2|\gamma_2-\gamma_1|^2}{\rho_1^{-1}f_1^{-1}+\rho_2^{-1}f_2^{-1}-h\omega^2+d^{(v)}-d^{(b)}}, \quad (29)$$

$$f_{1,2} \equiv f\left(\frac{\omega}{2\Delta_{1,2}}\right), \quad (30)$$

$$f(x) \equiv \frac{\arcsin(x)}{x\sqrt{1-x^2}}, \quad (31)$$

$$h \equiv -\frac{D_{11}^{(p)}D_{12}^{(p)}-(D_{12}^{(p)})^2}{4D_{12}^{(p)}\Delta_1\Delta_2}, \quad (32)$$

$$d^{(v)} \equiv -(D_{11}^{(v)}+D_{22}^{(v)}-2D_{12}^{(v)}), \quad (33)$$

$$d^{(b)} \equiv -2(D_{11}^{(b)}+D_{22}^{(b)}-2D_{12}^{(b)}). \quad (34)$$

The screening correction gives zero, as it must for $q=0$. See the Appendix.

It is a convenient, but incorrect, assumption that final-state interactions can be neglected. Almost all authors do not make any corrections: pairing, vertex, or bubble, represented above by nonzero $D_{ij}^{(p)}$, $D_{ij}^{(v)}$, and $D_{ij}^{(b)}$.[15] When these quantities are set equal to zero, we obtain

$$\chi_\gamma^0(\omega,q=0) = \frac{-2|\gamma_2-\gamma_1|^2}{\rho_1^{-1}f_1^{-1}+\rho_2^{-1}f_2^{-1}}. \quad (35)$$

This is identical to the result that would be obtained by using the expression *with* screening, Eq. (28), but with $\boldsymbol{R}^{(p,v,b)}(\omega,0)$ replaced by the bare response-function matrix $\boldsymbol{R}^0(\omega,0)=-2\|\boldsymbol{F}(\omega,0)\boldsymbol{\rho}\|$. The difference between $\chi_\gamma(\omega,q=0)$ and $\chi_\gamma^0(\omega,q=0)$ is both quantitative and qualitative.

VI. APPLICATION TO Fe PNICTIDES

Whereas the $q=0$ assumption is not realistic for MgB_2, it is for the Fe pnictides, magnetic superconductors with a lay-

ered structure that makes them nearly two dimensional, with very small components of the Fermi velocities perpendicular to the layers. For them, we apply Eqs. (29)–(34) to the two-band model with extended *s*-wave symmetry considered by Chubukov *et al.*[16] Those authors assume that $\Delta_2=-\Delta_1=-\Delta$ and $\rho_1=\rho_2=\rho$. In their notation, our matrices describing pairing, vertex, and bubble corrections would read

$$\boldsymbol{D}^{(p)}=\rho^{-1}\begin{bmatrix} u_4 & u_3 \\ u_3 & u_4 \end{bmatrix}; \quad \boldsymbol{D}^{(v)}=\rho^{-1}\begin{bmatrix} u_4 & u_2 \\ u_2 & u_4 \end{bmatrix};$$

$$\boldsymbol{D}^{(b)}=\rho^{-1}\begin{bmatrix} u_4 & u_1 \\ u_1 & u_4 \end{bmatrix}. \tag{36}$$

We then find

$$\chi_\gamma(\omega,q=0)=\frac{-|\gamma_2-\gamma_1|^2\rho f\left(\frac{\omega}{2\Delta}\right)}{1-\left(u_{eff}+\frac{\omega^2(u_4^2-u_3^2)}{8\Delta^2 u_3}\right)f\left(\frac{\omega}{2\Delta}\right)},$$

$$u_{eff}\equiv 2u_1-u_2-u_4. \tag{37}$$

Using renormalization-group arguments, Chubukov *et al.* asserted that u_{eff} is dominated by u_1 and is positive. This means that among all final-state interactions, the dominant one is repulsive, and it couples p/h pairs in one band to those in the other band. They assigned the value 0.4 to u_{eff}. If $\frac{\omega^2(u_4^2-u_3^2)}{8\Delta^2 u_3}$ is neglected with respect to u_{eff}, our result becomes similar to theirs,

$$\chi_\gamma(\omega,q=0)=-\frac{|\gamma_2-\gamma_1|^2\rho f\left(\frac{\omega}{2\Delta}\right)}{1-u_{eff}f\left(\frac{\omega}{2\Delta}\right)}. \tag{38}$$

When plotted, Im $\chi_\gamma(\omega+i0^+,0)$ for $u_{eff}=0.4$ is similar to the plot shown in their Fig. 1(b). There is a difference. Based on an argument involving an energy-dependent cutoff of the effective interaction, they used $f(\frac{\omega}{2\Delta})-1$ in place of our $f(\frac{\omega}{2\Delta})$. This replacement would give incorrect results if applied to the ideal limit to be discussed next.

VII. TWO-BAND CASE WITH FINITE WAVE VECTOR IN THE IDEAL LIMIT

Following Leggett,[3] we consider the case where the material parameters and regions of interest are such that ω and qv_j are both assumed to be nonzero but small compared with Δ_j. This leads to the approximations

$$F_j\cong Q_j\cong 1; \quad P_j\cong 1-\left(\frac{qc_j}{\omega}\right)^2, \tag{39}$$

where

$$c_j^2\equiv v_j^2\langle u_{k_j}^2\rangle_{FS}=\frac{v_j^2}{3}. \tag{40}$$

The last equality results from the assumption that the Fermi surface is spherical. With these assumptions, Eqs. (27) and (24) lead to the result

$$\boldsymbol{R}^{(p,v,b)}(\omega,q)=\frac{-2}{\left(\|\boldsymbol{\rho}^{-1}\|-\frac{\boldsymbol{I}\omega^2}{4\boldsymbol{U}+q^2\|\boldsymbol{c}^2\boldsymbol{\rho}\|}\right)-\boldsymbol{D}^{(v)}+2\boldsymbol{D}^{(b)}}. \tag{41}$$

Recall that $\|\boldsymbol{\rho}^{-1}\|$ and $\|\boldsymbol{c}^2\boldsymbol{\rho}\|$ denote diagonal matrices. This gives the following results from Eq. (28):

$$\chi_\gamma(\omega,q)=B_{\gamma^*,\Lambda\gamma}(\omega,q)=\frac{8|\gamma_2-\gamma_1|^2(\omega_o^2+v_o^2q^2)/V_o}{\omega^2-\omega_o^2-q^2v_o^2}, \tag{42a}$$

$$\omega_o^2\equiv-\frac{V_o 8D_{12}^{(p)}\Delta_1\Delta_2}{D_{11}^{(p)}D_{22}^{(p)}-(D_{12}^{(p)})^2}, \tag{42b}$$

$$v_o^2\equiv\frac{V_o\rho_1\rho_2c_1^2c_2^2}{\rho_1c_1^2+\rho_2c_2^2}, \tag{42c}$$

$$V_o\equiv\frac{1}{\rho_1}+\frac{1}{\rho_2}+d^{(v)}-d^{(b)}. \tag{42d}$$

[Recall Eqs. (33) and (34).] We derive from the denominator of Eq. (42a) the existence of a collective mode at an energy $\omega=\omega_L(q)$ obeying

$$\omega_L^2(q)\equiv\omega_o^2+v_o^2q^2 \tag{43}$$

with an energy (mass) ω_o and a dispersion velocity v_o. These are generalizations of the results given by Leggett[3] in his Eq. (3.39). If our parameter V_o were given by $V_o\equiv\rho_1^{-1}+\rho_2^{-1}$, and taking into account the fact that our density of states ρ_i is for one spin, whereas his is for both spins, we would obtain his result. Thus, setting $\boldsymbol{D}^{(v)}=\boldsymbol{D}^{(b)}=0$, i.e., the absence of a vertex correction in the particle/hole channel and of a bubble correction, gives his results for the mode frequency and its dispersion with q.

Use of Eqs. (11) and (42a) gives us an analytical result for the Raman intensity in this ideal case. If $\omega\leq\omega_o$, $I_{ideal}(\omega)=0$. If $\omega>\omega_o$,

$$I_{ideal}(\omega)=\frac{S_{fqi}16q''\omega^2\Phi(q',q'',\omega)}{(\rho_1+\rho_2)V_ov_o\sqrt{\delta\omega^2}}, \tag{44a}$$

$$\Phi(q',q'',\omega)\equiv\frac{q'^2+q''^2+v_o^{-2}\delta\omega^2}{[q'^2+q''^2+v_o^{-2}\delta\omega^2]^2-4v_o^{-2}\delta\omega^2q'^2}, \tag{44b}$$

TABLE I. Values of input parameters used in the calculation for MgB_2. Here "Ry" denotes the Rydberg and "c" means "unit cell." To convert the units of the product of q'' with v_1 into millielectron volt, multiply by $\hbar = 0.658 \times 10^{-12}$ meV s.

Name	D_{11}	D_{22}	D_{12}	ρ_1	ρ_2	
Value	−0.47	−0.1	−0.08	2.04	2.78	
Units	Ry-c	Ry-c	Ry-c	/Ry-spin-c	/Ry-spin-c	
Name	Δ_1	Δ_2	v_1	v_2	q'	q''
Value	6.75	2.3	0.38	4.7	1.73	4.18
Units	meV	meV	10^5 m/s	10^5 m/s	10^7 m^{-1}	10^7 m^{-1}

$$\delta\omega^2 \equiv \omega^2 - \omega_o^2, \quad S_{fqi} \equiv \frac{|\gamma_2 - \gamma_1|^2(\rho_1 + \rho_2)}{4q''}. \tag{44c}$$

S_{fqi} is introduced as a scale factor for this situation where an integral has been performed over q. The quantity $I_{ideal}(\omega)/S_{fqi}$ is dimensionless.

VIII. APPLICATION TO MAGNESIUM DIBORIDE

For MgB_2 the superconducting pairing comes primarily from optical phonons and is attractive.[17] The intra σ band pairing potential $D_{11}^{(p)}$ is due to modes that become the doubly degenerate optical phonon of E_g symmetry at $q \approx 0$ wherein the two B atoms in the unit cell move perpendicular to the c axis. The intra π band pairing potential $D_{22}^{(p)}$ and inter π-σ band pairing potential $D_{12}^{(p)}$ are due to the mode that becomes the optical phonon of B_{1g} symmetry at $q \approx 0$ wherein the B atoms move parallel to the c axis. Neither of these phonons for the relatively small (with respect to the inverse lattice constant) physical values of q are capable of making a contribution to the bubble correction because the lines connecting the bubbles are, in fact proportional to phonon propagators and they must have the same symmetry, A_{1g}, as that of the bare Raman vertex. Thus $\boldsymbol{D}^{(b)}$ can only be due to the much weaker effects of A_{1g} symmetry acoustical phonons. We thus assume $\boldsymbol{D}^{(b)} = 0$. On the other hand, for pairing and for the vertex correction, no such symmetry arguments apply, and we simply assume that $\boldsymbol{D}^{(v)} = \boldsymbol{D}^{(p)} = \boldsymbol{D}$.

The material parameters used by Blumberg *et al.*[7] are those shown in Table I. The values of q'' and q' are estimates based on optical data.[10] The other parameters are from Liu *et al.*[4] Using these parameters, we calculate $\omega_o = 12.42$ meV and $v_o = 0.23 \times 10^5$ m/s. This value of ω_o is much too large for the conditions of the ideal limit to be satisfied. Note that roughly $\omega_o \propto \sqrt{-D_{12}}$ and that v_o depends very weakly on $-D_{12}$ as long as $-2D_{12} \ll \rho_1^{-1} + \rho_2^{-1} - D_{11} - D_{22}$, which is the case here. For example, if $-D_{12}$ were to equal 0.001 Ry cell, we would have $\omega_o = 1.37$ meV, less than $2\Delta_2$, and the ideal limit would amount to a good approximation.

IX. REAL CASE

We now turn to the more realistic case, where F_j, Q_j, and P_j have complicated dependences on ω and q. They depend on the properties of $f(\beta) \equiv \frac{\arcsin \beta}{\beta\sqrt{1-\beta^2}}$ as a function of $\beta = \beta_j(q,u,\omega) \equiv \sqrt{\frac{\omega^2 - (qv_j u)^2}{4\Delta_j^2}}$. Keeping in mind that ω has an infinitesimally small positive imaginary part, we may write for various regions,

$$f(\beta) = -\frac{\ln(\sqrt{1+|\beta|^2} - |\beta|)}{|\beta|\sqrt{1+|\beta|^2}}, \quad \text{when } \beta^2 < 0, \tag{45a}$$

$$f(\beta) = \frac{\arcsin(\beta)}{\beta\sqrt{1-\beta^2}} = \frac{\frac{\pi}{2} - \arcsin(\sqrt{1-\beta^2})}{\beta\sqrt{1-\beta^2}}, \quad \text{when } 0 \le \beta < 1, \tag{45b}$$

$$f(\beta) = \frac{\ln(\beta - \sqrt{\beta^2 - 1})}{\beta\sqrt{\beta^2 - 1}} + \frac{\pi i/2}{\beta\sqrt{\beta^2 - 1}}, \quad \text{when } \beta > 1. \tag{45c}$$

These expressions are to be inserted into Eqs. (14) and (15). We replace β with $(2\Delta_j)^{-1}\sqrt{\omega^2 - (qv_j u)^2}$ and then average over u to obtain $F_j(q,\omega)$, $Q_j(q,\omega)$, and $P_j(q,\omega)$. The u integrals yield elliptic integrals for the imaginary parts but we know of no analytic forms for the real parts. We chose not to rely on numerical integration to obtain the real parts of F, P, and Q. Instead we approximate the real parts of f, p, and r with functions of β that can be averaged over u. We used the following approximate functions for the real part of $f(\beta)$. For $\beta^2 < 0$, $0 \le \beta \le \frac{1}{\sqrt{2}}$, $\frac{1}{\sqrt{2}} \le \beta < 1$, and $\beta > 1$, respectively, we used

$$f^{(0)}(\beta) \equiv \frac{7}{3(1-\beta^2)} - \frac{3}{(1-\beta^2)^2} + \frac{5}{3(1-\beta^2)^4}, \tag{46a}$$

$$f^{(1)}(\beta) \equiv \frac{1 + \frac{1}{6}\beta^2 + \beta^4\left(-\frac{13}{3} + \sqrt{2}\pi\right)}{\sqrt{1-\beta^2}}, \tag{46b}$$

$$f^{(2)}(\beta) \equiv \frac{\frac{\pi}{2}}{\beta\sqrt{1-\beta^2}} - f^{(1)}(\sqrt{1-\beta^2}), \tag{46c}$$

$$f^{(3)}(\beta) \equiv \frac{-\frac{5}{6}-\frac{1}{2}\ln(\beta^2)}{\beta^2} - \frac{1}{6\beta^4}. \tag{46d}$$

These have the properties that $f^{(0)}(\beta)$ and $f^{(1)}(\beta)$ tend to 1 as β^2 tends to 0 from below and above, respectively; $f^{(2)}(\beta)$ has the same limiting, singular behavior as $f(\beta)$, when β tends to 1 from below; and $f^{(3)}(\beta)$ tends to the correct limit, -1, when β tends to 1 from above. Moreover, the approximations $f^{(1)}(\beta)$ and $f^{(2)}(\beta)$ agree when $\beta=1/\sqrt{2}$. These approximations for $f(\beta)$ were inserted in Eqs. (14) and (15) to obtain approximate, integrable, versions of the real parts of $p(\beta)$ and $r(\beta)$. The averages over u were than calculated analytically with the help of "Mathematica." The resulting functions F_j, P_j, and Q_j of q and ω were used in Eqs. (24), (27), and (28) to calculate analytically $\mathrm{Im}[B_{\Lambda(\gamma),\gamma^*}(q,\omega+i0^+)] = \mathrm{Im}[\chi_\gamma(q,\omega+i0^+)]$ that was inserted into Eq. (11) for numerical integration over q from 0 to an upper limit of $10q''$ that was sufficiently large to be accurate in the peak region of the intensity plots.

X. NUMERICAL RESULTS

We start by comparing in Fig. 1 the ideal case results for $-D_{12}=0.001$, 0.003, and 0.01 with the real case result for the unrealistically small value of $-D_{12}=0.01$.

Note the similarity of the two $-D_{12}=0.01$ spectra. Note also the discontinuity at $\omega=2\Delta_2=4.6$ meV for the real case. For more realistic values of $-D_{12}$ the effect of departure of the functions F_j, P_j, and Q_j from their ideal case forms leads to dramatic changes in the Raman spectra, as shown in Fig. 2. Note that the discontinuity at $\omega=2\Delta_2$ is now joined by one at $\omega=2\Delta_1=13.5$ meV.

Table I gives a calculated value for $-D_{12}$ of 0.08. The experimental result of Blumberg *et al.*[7] shows that the peak occurs at 9.4 meV. Our calculation with $-D_{12}=0.08$ gives the peak energy at 9.0 meV whereas our calculation with $-D_{12}=0.10$ has a peak energy very close to the experimental value. Taken together, the results in Figs. 1 and 2 show how the collective mode, first predicted by Leggett, but corrected for final-state interactions, evolves into a resonance mode peaked very close to the energy found by the Raman experiment as the parameter $-D_{12}$ increases from very small values to those close to the LDA result.

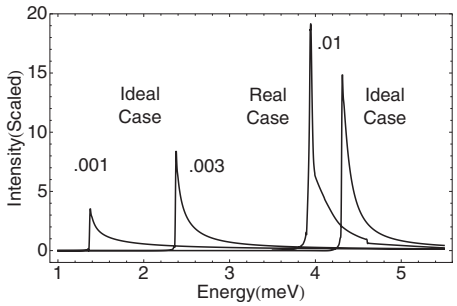

FIG. 1. Scaled Raman intensity for the ideal case with interband pairing potential $-D_{12}=0.001$, 0.003, and 0.01. The singularity at each peak was rounded. Also shown is the real case result for $-D_{12}=0.01$. Here, a small positive imaginary part was added to the energy variable ω.

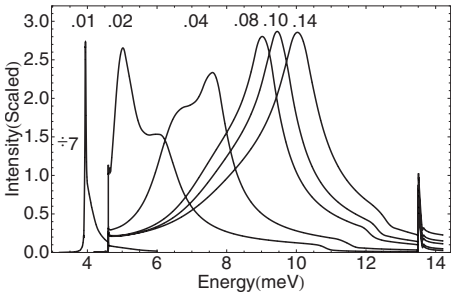

FIG. 2. Scaled Raman intensity for the real case for $-D_{12}=0.01$, 0.02, 0.04, 0.08, 0.10, and 0.14. For the 0.01 plot, a small positive imaginary part was added to the energy variable ω. "Wiggles" near 4.6 and 13.5 meV, the values of the two gaps, $2\Delta_1$ and $2\Delta_2$, are artifacts of smoothing the numerical integration carried out at a discreet number of points.

We show a final comparison in Fig. 3(b), namely, between the $-D_{12}=0.10$ result from Fig. 2 and the result with the same value of $-D_{12}$ obtained by setting $q=0$. The effect of

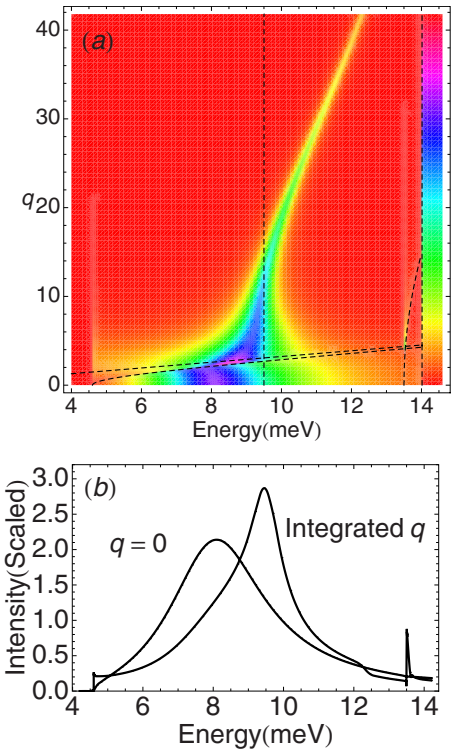

FIG. 3. (Color online) Results for the interband pairing potential $-D_{12}=0.10$. (a) Density plot of the integrand in Eq. (11) with values of q (in units of 10^7 m^{-1}) extending to $10q''$. Intensity scale is shown by the color bar on the right. The dashed curve starting at 4.6 meV obeys $\hbar v_\pi k=\sqrt{\omega^2-4\Delta_\pi^2}$. The dashed slanted straight line obeys $\hbar v_\pi k=\omega$, and the dashed curve starting at 13.5 meV obeys $\hbar v_\sigma k=\sqrt{\omega^2-4\Delta_\sigma^2}$. (b) The Integrated q plot is the same as the $-D_{12}=0.10$ plot in Fig. 2. The vertical dashed line at 9.5 meV in (a) denotes the value of Energy where the Integrated q plot has its maximum. The "$q=0$" plot is equivalent to a $q=0$ cut along the lower edge of the density plot in (a).

finite values of q on shifting up the energy of the peak is obvious. This is a kinematic effect that crudely results from the need for higher values of ω to compensate for nonzero values of $(q\cdot v_k)^2$ in Eqs. (1), (14), and (15).

These effects play out in an interesting way in our case where the two Fermi velocities differ by a factor of 12. The peak of $-\mathrm{Im}[\chi_\gamma(q,\omega)]$ moves from 8 meV at $q=0$ to *lower* energy as q increases from 0 to about 2×10^7 m^{-1}. Then the peak moves to higher energy. The behavior of the integrand in Eq. (11) can be seen in the density plot in Fig. 3(a).

Note that the shoulder at 12.3 meV in the "Integrated q" curve of Fig. 3(b) corresponds to the peak at the $q=10q''$ cut at the top of the density plot of Fig. 3(a). If we were to extend the upper limit of the integral over q beyond $10q''$, this shoulder would move up in energy but there would be no effect in the shape of the Integrated q plot in the energy range between 4.6 and 11.5 meV. The dispersion of the peak in the density plot with wave vector q beyond about 10^8 m^{-1} is caused by the nonzero, but small, nature of the velocity v_σ. If we had set $v_\sigma=0$, the peak in the Integrated q plot would occur at 9 meV, and it would be higher and narrower than in the plot shown in Fig. 3(b).

Recall that we had set $\mathbf{D}^{(v)}=\mathbf{D}^{(p)}\neq0$ and $\mathbf{D}^{(b)}=0$ to obtain these results. Had we set $\mathbf{D}^{(v)}=0$ and $\mathbf{D}^{(b)}=0$, the resulting Raman intensity calculation would give a peak at a lower energy. In particular, the peak features shown in the density plot in Fig. 3(a) would occur at energies 1.5–2 meV lower. Had we used $\mathbf{D}^{(v)}=\mathbf{D}^{(p)}=\mathbf{D}^{(b)}\neq0$, they would have occurred at still lower energies.

XI. DISCUSSION

To the author's knowledge this work amounts to the first attempt at a full treatment of finite wave-vector effects in the calculation of electronic Raman scattering in a superconductor. Our real case calculation takes these effects into account only through the use of the toy model assumption of spherical Fermi surfaces together with approximations to the real part of $f(\beta)$ [Eqs. (46a)–(46d)]. A more realistic calculation would involve a much more complex model of the Fermi surfaces and a great deal more massive numerical calculation. Nevertheless, the toy model used here seems to have captured the essential features of Leggett's mode as applied to the real multiband superconductor MgB_2: damping due to decay into the π band(s) and finite wave-vector effects in both π and σ bands.

When applied to the normal state, our model does not account quantitatively or qualitatively for the experimental results in A_{1g} symmetry.[7] The data show a rising continuum in both A_{1g} and E_{2g} symmetries that is cutoff below $2\Delta_\pi$ in the superconducting state. An explanation will require a model for the bare vertex γ_k that goes beyond the scope of the present work.

ACKNOWLEDGMENTS

The author thanks Girsh Blumberg for sharing his Raman data on MgB_2 and for his insight that the experimental A_{1g} peak at 9.4 meV was the manifestation of Leggett's collective mode in a real multiband superconductor. He also thanks Tony Leggett for discussions and a key question. The answer convinced the author that, in principle, the bubble correction needs to be considered in the context of electronic Raman scattering.

APPENDIX: FLOW, COUNTERFLOW, AND THE SCREENING CORRECTION

Here we derive an important result that has rather general applicability. It concerns the interplay between the correction for pairing and the screening correction when the wavevector q is zero. In that case we have

$$r_k(\omega,0)=p_k(\omega,0)=f_k(\omega,0)\equiv\frac{\arcsin\left(\frac{\omega}{2\Delta_k}\right)}{\frac{\omega}{2\Delta_k}\sqrt{1-\left(\frac{\omega}{2\Delta_k}\right)^2}}.$$

All the factors in square brackets in Eqs. (4), (5), and (7) become $f_{k'}(\omega,0)[\Gamma^{(2)}_{k'}(\omega,0)-2i\Delta_{k'}\omega^{-1}\Gamma^{(3)}_{k'}(\omega,0)]$.

To examine the implications for screening, we need to know the behavior of $\Gamma^{(2,3)}_{k,1}(\omega,0)$, where the second subscript denotes the value of $\gamma_k=1$. We find that setting

$$\Gamma^{(2)}_{k,1}(\omega,0)=2i\Delta_k\omega^{-1}\ \text{ and }\ \Gamma^{(3)}_{k,1}(\omega,0)=1,$$

thus making $[\Gamma^{(2)}_{k',1}(\omega,0)-2i\Delta_{k'}\omega^{-1}\Gamma^{(3)}_{k',1}(\omega,0)]=0$, trivially satisfies both Eq. (4) and [with the help of Eq. (6)] Eq. (5). These results show that the term in square brackets vanishes for each k on the right side of Eq. (7) for $B_{\gamma',\Gamma1}(\omega,0)$. Thus, $B_{\gamma',\Gamma1}(\omega,0)=0$ for any γ'_k.

Of the two terms in square brackets in Eq. (7), the $\Gamma^{(3)}_k$ term can be thought of as "flow" of a k-dependent longitudinal particle/hole current, and the $\Gamma^{(2)}_k$ term as a k-dependent particle/particle "counterflow" current produced in response to the p/h current. For each value of k, p/p, and p/h currents tend to cancel, and, when the p/h current is uniform in k space ($\gamma_k\propto1$), we have just shown that this cancellation is exact for each k. At a deeper level the result $\Gamma^{(2)}(1)=2i\Delta\omega^{-1}$ is a result of gauge invariance and particle conservation. For example, see the first of Nambu's Eq. (7.6).[11]

For nonzero $\boldsymbol{q}$, Eqs. (4), (5), and (7) apply with $p_k(\omega,\boldsymbol{q})-f_k(\omega,\boldsymbol{q})$ and $r_k(\omega,\boldsymbol{q})-f_k(\omega,\boldsymbol{q})\neq0$, and for small q, the leading terms in an expansion are $\propto q^2$. This has the consequence that the leading term in an expansion of $B_{\gamma',\Gamma1}(\omega,\boldsymbol{q})$ is $\propto q^2$. This also applies to $B_{\gamma^*,\Gamma1}(\omega,\boldsymbol{q})$, $B_{1,\Gamma\gamma}(\omega,\boldsymbol{q})$, and $B_{1,\Gamma1}(\omega,\boldsymbol{q})$ in the screening correction. [See Eqs. (9a) and (10).] Thus, the leading term in an expansion of the screening correction is $\propto q^2$.

We have shown that the screening correction gives zero in the $q=0$ limit. We have sketched the proof here for the case of nonretarded interactions restricted to the Fermi surface. A similar proof involving vertex corrections, bubble corrections, and screening should be possible for nonretarded interactions not restricted to the Fermi surface. Because of the underlying connection to gauge invariance, this statement

about the screening correction should hold with retarded interactions as well.

Thus, for A_{1g} symmetry and $q=0$, it is not correct to use the bare bubble, Eq. (7), $B_{\gamma',\gamma}(\omega,0)=-2\int dS_k \gamma'_k f_k(\omega,0)\gamma_k$, in the bare version of the screening correction, Eq. (10), with $\Gamma_1 \to 1$ and $\Gamma_\gamma \to \gamma$. One must have a solvable model for the pairing interaction $[D^{(p)}(k,k')]$ and the vertex correction $[D^{(v)}(k,k')]$, and then solve equations like Eqs. (4) and (5) to obtain expressions for $\Gamma^{(2)}_{k,\gamma}(\omega,0)$ and $\Gamma^{(3)}_{k,\gamma}(\omega,0)$ to use in Eq. (7). One way to do this would involve a reinterpretation of our solution for the multiband case. One can interpret matrix Eqs. (17)–(21) as resulting from a fine scale, or large n, discrete version of Eqs. (4)–(7). The solutions are given by Eqs. (22)–(27). The response-function matrices $\boldsymbol{R}^{(p)}(\omega,q)$, $\boldsymbol{R}^{(p,v)}(\omega,q)$, and $\boldsymbol{R}^{(p,v,b)}(\omega,q)$ are symmetric. They can be shown to have the property that $\mathbf{1}\cdot\boldsymbol{R}(\omega,q)=\boldsymbol{R}(\omega,q)\cdot\mathbf{1}\propto q^2$ for small q.

Another solvable model results from using the product ansatz $D^{(p)}_{jj'}\propto\Delta_j\Delta_{j'}$. To obtain a solution, Eqs. (19) and (20) must first be left multiplied by $\boldsymbol{D}^{(p)}=\boldsymbol{W}^{-1}$.

[1] N. N. Bogolyubov, V. V. Tolmachev, and D. N. Shirkov, *A New Method in the Theory of Superconductivity* (Consultants Bureau, New York, 1959).

[2] P. W. Anderson, Phys. Rev. **110**, 827 (1958); **112**, 1900 (1958).

[3] A. J. Leggett, Prog. Theor. Phys. **36**, 901 (1966).

[4] A. Y. Liu, I. I. Mazin, and J. Kortus, Phys. Rev. Lett. **87**, 087005 (2001).

[5] P. Szabo, P. Samuely, J. Kacmarcik, T. Klein, J. Marcus, D. Fruchart, S. Miraglia, C. Marcenat, and A. G. M. Jansen, Phys. Rev. Lett. **87**, 137005 (2001); M. Iavarone, G. Karapetrov, A. E. Koshelev, W. K. Kwok, G. W. Crabtree, D. G. Hinks, W. N. Kang, E.-M. Choi, H. J. Kim, H.-J. Kim, and S. I. Lee, *ibid.* **89**, 187002 (2002); S. Tsuda, T. Yokoya, T. Kiss, Y. Takano, K. Togano, H. Kito, H. Ihara, and S. Shin, *ibid.* **87**, 177006 (2001); S. Souma, Y. Machida, T. Sato, T. Takahashi, H. Matsui, S.-C. Wang, H. Ding, A. Kaminski, J. C. Campuzano, S. Sasaki, and K. Kadowaki, Nature (London) **423**, 65 (2003).

[6] A. Mialitsin, B. S. Dennis, N. D. Zhigadlo, J. Karpinski, and G. Blumberg, Phys. Rev. B **75**, 020509(R) (2007).

[7] G. Blumberg, A. Mialitsin, B. S. Dennis, M. V. Klein, N. D. Zhigadlo, and J. Karpinski, Phys. Rev. Lett. **99**, 227002 (2007).

[8] M. V. Klein and S. B. Dierker, Phys. Rev. B **29**, 4976 (1984).

[9] A. Kawabata, J. Phys. Soc. Jpn. **30**, 68 (1971).

[10] V. Guritanu, A. B. Kuzmenko, D. van der Marel, S. M. Kazakov, N. D. Zhigadlo, and J. Karpinski, Phys. Rev. B **73**, 104509 (2006).

[11] Y. Nambu, Phys. Rev. **117**, 648 (1960).

[12] One can prove Eq. (8) by iterating Eqs. (4) and (5), starting with $\Gamma^{(3)}_{k,\gamma}(\omega,\boldsymbol{q})=\gamma_k$ and $\Gamma^{(2)}_{k,\gamma}(\omega,\boldsymbol{q})=0$. The result will give an infinite series for $B_{\gamma',\Gamma\gamma}(\omega,\boldsymbol{q})$, each term of which is symmetric in the components of γ and γ'.

[13] Note that this assumption rules out the simplifying product ansatz of the form $D^{(p)}_{j,j'}\propto\Delta_j\Delta_{j'}$.

[14] The necessity for including bubble diagrams was mentioned by Nambu (Ref. 11) in another context, but was not considered by K-D (Ref. 8).

[15] One exception is the paper by Chubukov *et al.* See the next reference.

[16] A. V. Chubukov, I. Eremin, and M. M. Korshunov, Phys. Rev. B **79**, 220501(R) (2009).

[17] A. Shukla, M. Calandra, M. d'Astuto, M. Lazzeri, F. Mauri, C. Bellin, M. Krisch, J. Karpinski, S. M. Kazakov, J. Jun, D. Daghero, and K. Parlinski, Phys. Rev. Lett. **90**, 095506 (2003); J. Geerk, R. Schneider, G. Linker, A. G. Zaitsev, R. Heid, K.-P. Bohnen, and H. v. Lohneysen, *ibid.* **94**, 227005 (2005).